PROCEEDINGS OF SCIENCE

In-depth analysis of selected major solar events with the HEPP-L particle detector onboard CSES-01 in low-Earth orbit

Alessio Perinelli[a,b,*] **and Francesco M. Follega**[a,b] **on behalf of the CSES-Limadou collaboration**

[a] *Department of Physics, University of Trento, via Sommarive 14, 38122 Trento, Italy*
[b] *TIFPA-INFN, University of Trento, via Sommarive 14, 38122 Trento, Italy*

E-mail: alessio.perinelli@unitn.it, francesco.follega@unitn.it

The characterization of the effects of solar disturbances on the Earth's ionosphere is crucial for the monitoring and understanding of space weather. While satellites orbiting outside of the Van Allen belts allow for direct measurements of the ejected particles and of magnetic field perturbations, low Earth orbit spacecraft, such as the China Seismo-Electromagnetic Satellite (CSES-01), provide a direct assessment of the effect of these events on the Earth ionosphere. Here we present a detailed study of proton flux perturbations measured by the High-Energy Particle Package (HEPP-L) onboard CSES-01 during two major, prototypical solar events: the ground-level enhancement (GLE) of 2021-10-28, and an X3.3 flare occurred on 2024-02-09. The analysis of fluxes measured by HEPP-L, capable of detecting 2 MeV-20 MeV protons, relies on a robust statistical approach to model the expected background flux in ordinary conditions and identify anomalies attributable to space weather events. For the case studies outlined above, upon identification of anomalies, we assess the properties of the excess proton flux, including the temporal evolution of its spectral features. These results enrich the present knowledge of the effects of solar activity on the Earth's ionosphere, demonstrating the crucial role that the CSES mission can play in space weather studies.

39th International Cosmic Ray Conference (ICRC2025)
15–24 July 2025
Geneva, Switzerland

ICRC 2025
The Astroparticle Physics Conference
Geneva July 15-24, 2025

*Speaker

PoS(ICRC2025)1354

1. Introduction

The CSES (China Seismo-Electromagnetic Satellite) mission is a scientific collaboration between Italy and China aimed to the construction of multi-satellite and multi-payload space observatory with multifaceted goals, as highlighted by the variety of payloads hosted onboard: particle detectors, electric and magnetic field detectors, as well as several instruments dedicated to the characterization of the plasma environment. While the primary task of the mission is to investigate seismic-induced perturbations of the ionosphere [1], CSES payloads also allow to study cosmic rays [2], gamma ray bursts [3, 4], and space weather phenomena [5–7]. The first satellite was launched on the February 2, 2018 and is still operative, while the second was recently launched from the Chinese launch center of Jiayuguan on the 14th of June 2025.

The CSES constellation provides valuable data during the occurrence of space weather events. Specifically, by leveraging on the on-board particle detector payloads, it can help characterizing the impact of solar events on the complex environment of the Earth's ionosphere, complementary to measurements carried out by observatories at higher altitudes or orbiting the Sun. These observations are crucial to investigate the complex interplay between magnetosphere and ionosphere during geomagnetic storms [6, 8].

In this work we present an analysis concept aimed at characterizing the effect of solar events on the near-Earth environment by exploiting particle data collected by one of the particle detectors on board the CSES-01 satellite, namely the High-Energy Particle Package (HEPP) [5]. By showcasing the results on four selected major solar events, we illustrate the contribution that low-Earth orbiting observatories can play to enhance our understanding of the perturbations on particle populations induced by solar activity.

2. The HEPP-L detector onboard CSES-01

The CSES-01 satellite is the first spacecraft of the CSES constellation. CSES-01 flies on a sun-synchronous almost-polar orbit at 500 km altitude and passes over a given point roughly at local 2 PM (daytime, descending semi-orbits) or at local 2 AM (nighttime, ascending semi-orbits). The orbital period is approximately 94 minutes and the revisit time is 5 days. Payloads are switched off in the polar regions, above 65° and below −65° in geographic latitude, so no data are available therein.

The HEPP detector onboard CSES-01 consists of three sub-detectors [5]: the "low-energy" (HEPP-L) particle detector, considered in this work; a "high-energy" (HEPP-H) one; and an X-ray detector (HEPP-X). Passive collimators divide the HEPP-L field of view in nine directional channels, or "telescopes", with 5 narrow ones (13° opening angle) placed above 4 wide ones (30° opening angle). Both groups are placed along an arc oriented at about 70° from zenith and orthogonal to the flight direction. The active part of each channel is made of a pair of silicon detectors, a thin 300 μm one followed by a thick 2 mm one. A plastic scintillator shared by all channels acts as an anti-coincidence detectors. A diagram of the detector can be found in Ref. [3] (fig. 2 therein) and Ref. [9] (figs. 1,6 therein). Overall, HEPP-L is able to provide a measurement of electron fluxes between 0.1 MeV and 3 MeV, as well as proton fluxes between 2 MeV and 20 MeV. Flux measurements are provided for each channel in 256 energy bins, with a time resolution of 1 s.

In the present study, we considered proton flux data, and we excluded channels 6, 8 and 9, as they are characterized by higher noise and contamination by other physical processes. The considered data period goes from February 2019 to September 2024.

3. Blind search of anomalous events

The blind search is separately carried out for fluxes corresponding to each detector channel, each orbit direction (daytime and nighttime), and for each of the three considered energy intervals, namely $[2.5, 7)$ MeV, $[7, 12)$ MeV, and $[12, 20)$ MeV, over which proton fluxes are integrated. This energy re-binning is necessary to enhance the statistics, as well as to simplify the detection of anomalies, with respect to the original energy resolution.

3.1 Background modeling

The core of the present analysis consists in a blind search for anomalous fluxes persisting for several hours or days, as it is typical of solar event-related phenomena. The background modeling strategy, inherited from two previous works [4, 10], relies on the construction of maps of background flux on a uniform grid of $1^\circ \times 1^\circ$ in the geomagnetic latitude-longitude space. Each cell (i, j) is associated to a median flux $\bar{\Phi}_{(i,j)}$ and a related standard deviation $s_{(i,j)}$ computed from a set $\Phi_{n\,(i,j)}$ of flux values collected for that cell; each contributing value Φ_n corresponds to the mean flux of a single orbital passage through the cell. Orbital passages are considered only if the space weather conditions are deemed to be quiet according to the SYM-H index (see Appendix B of Ref. [10] for further details). For some of the grid cells, flux values are unavailable because of the incomplete satellite coverage at 1° resolution, or merely due to missing data. These missing values are reconstructed by relying on a spline interpolation using Steffen's method [11], which guarantees that no artificial maxima are introduced, over the neighboring cells at the same latitude. An example of background map for channel 1 in the energy range 2.5 - 7 MeV is shown in Fig. 1(b).

For the purpose of the blind search, we considered "signal" windows of 20 days sliding along the whole data period in steps of 10 days. Given a signal window centered in t_k and covering the interval $[t_k - 10\,\text{days}, t_k + 10\,\text{days}]$, the "background" window used to build the background flux map consists in the union of the 60 days-long intervals $[t_k - 70\,\text{days}, t_k - 10\,\text{days})$, $(t_k + 10\,\text{days}, t_k + 70\,\text{days}]$. The data period is covered by 194 signal windows, whose centers go from t_1 = 2019-04-01 00:00:00 UTC to t_{194} = 2024-07-13 00:00:00 UTC. A diagram of this time division approach is shown in Fig. 1(a).

3.2 Outlier detection and pruning

The measured flux at each second along a given orbit of a signal window is compared to the background in the corresponding cell of the background map. An "outlier" is defined as a sample for which the signal flux overcomes the median background flux by more than 20 times the background standard deviation. This threshold was tuned on the data to compensate for the strong variability of fluxes in the high-latitude regions, as well as to account for the highly non-normal distribution of background flux values.

The daily number of outliers as a function of time is displayed in Fig. 2(a) alongside the monthly sunspot number. Interestingly, the occurrence rate of outliers appears to be well correlated with the

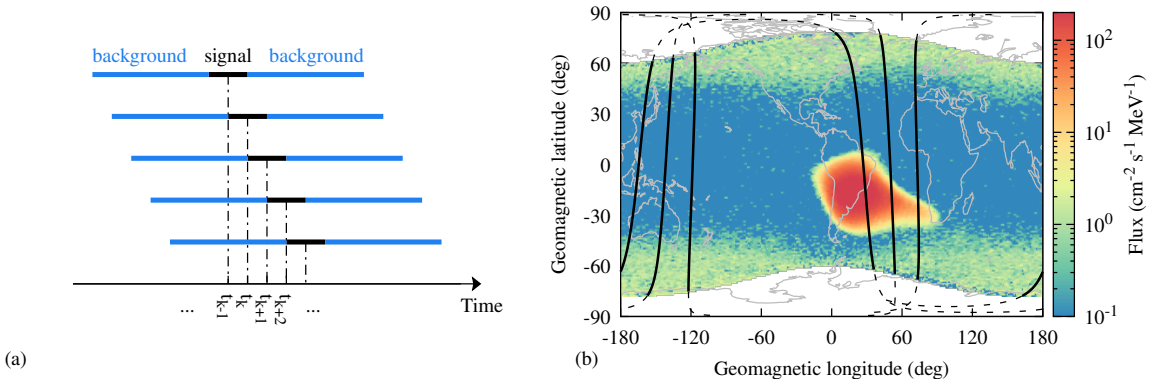

Figure 1: (a) Diagram of the time division approach for the detection of outliers within a signal window (black) according to the background model provided by the preceding and following background periods (blue). (b) Example of background map in geomagnetic coordinates, corresponding to the signal window centered at 2021-11-06 00:00:00 UTC. Data are displayed for protons in the energy range 2.5 - 7 MeV, using HEPP-L channel 1 . The black curves show the footprint of six example semi-orbits of CSES-01, distorted by the projection in geomagnetic coordinates; dashed lines correspond to the part of the orbit in which payloads are switched off.

sunspot number, suggesting that outliers are mainly stemming from perturbations linked to solar activity.

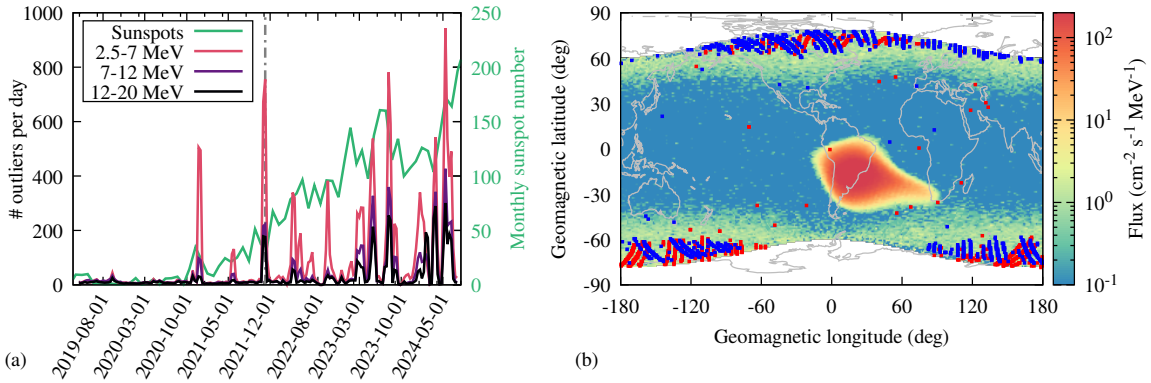

Figure 2: (a) Daily number of outliers as a function of the signal window central time t_k. Outliers are counted summing all channels and both semi-orbit directions. The vertical gray dash-dotted line corresponds to the signal window central time for which panel (b) is shown. (b) Spatial distribution of outliers superimposed to the background map for the signal window centered at 2021-11-06 00:00:00 UTC. Data are displayed for HEPP-L channel 1 and for the energy range 2.5 - 7 MeV. Each blue (red) dot corresponds to a single nighttime (daytime) outlier.

Figure 2(b) shows an example of the geographical location of outliers of channel 1 for a single signal window centered at 2021-11-06 00:00:00 UTC and a single energy range (2.5 - 7 MeV). Most outliers populate the high-latitude regions (beyond ±60°), although few sparse outliers are also present in the equatorial region.

The set of detected outliers (345538 in total) is refined by pruning out those within the geomagnetic latitude range $(-40°, 40°)$, as solar events are not expected to produce particle flux

anomalies within the equatorial region. Subsequently, temporally-sparse outliers, defined as outliers for which there is no other outlier within ±100 s, are removed[1]. After these selections, 294795 outliers (85.3%) are retained.

As a last step, outliers are assigned to clusters by relying on the DBSCAN algorithm of the scikit-learn Python library [12]. The DBSCAN algorithm operates on the temporal coordinate of outliers, joining together nighttime and daytime outliers, but separately for each energy range and channel. The distance parameter provided to the DBSCAN algorithm was set to 200 min, corresponding to approximately two orbital periods. Finally, outliers assigned to clusters with less than 10 elements are discarded. This condition corresponds to the request to have at least 10 seconds of outliers over approximately two orbits. The resulting set contains 264470 outliers divided into 1402 clusters, with approximately 50% of them stemming from the lowest energy range (2.5 - 7 MeV), 30% from the intermediate one (7 - 12 MeV), and 20% from the highest energy range (12 - 20 MeV).

3.3 Association to solar event and spectral evaluation

Clusters obtained through the procedure described so far are matched to a catalog of solar flares with an associated halo CME. Given the flare timestamp, we look for clusters starting after the timestamp and within 24 hours of it. If a cluster is found within this time period for at least three channels out of six (strong direction dependence in these event is not expected for low energy particles), the event is deemed to be detected by HEPP-L and all the found clusters are associated to it. The set of associated clusters is then extended by including all successive clusters until all channels are "quiet", i.e. do not provide any cluster, for more than 24 hours.

Although the division in three energy ranges already provides valuable information on the energetic distribution of anomalous protons, a spectral characterization is carried out after association with solar events, as follows. Taking into account all outliers that make up the clusters associated to a given event, and for each cell of the $1^\circ \times 1^\circ$ grid in which at least one outlier lies, we collect the average measured flux both within the signal time window and the background time windows. These fluxes are re-binned in 16 energy bins out of the 256 original ones to mitigate the lack of sufficient statistics. Finally, in order to summarize the information of all the grid cells exhibiting outliers, the fluxes are further averaged by putting together all cells belonging to the same latitude "stripe", defined as intervals of 5° in geomagnetic latitude.

4. Selected showcase events

4.1 GLE of 2021-10-28

The event starts with a X-1.0 flare with halo CME in region AR12887 at 2021-10-28 15:17 UTC. Between Oct. 28 and Nov. 9, seven subsequent M-class flares were detected. Figure 3 shows the detected outliers and clusters associated to this event, as well as the corresponding latitudinal distribution and spectra. The detected outliers cover about 200 hours after the reference UTC of the flare.

[1] A temporal window of ±100 s approximately corresponds to a distance along the orbit of $\sim 6.4^\circ$ in latitude.

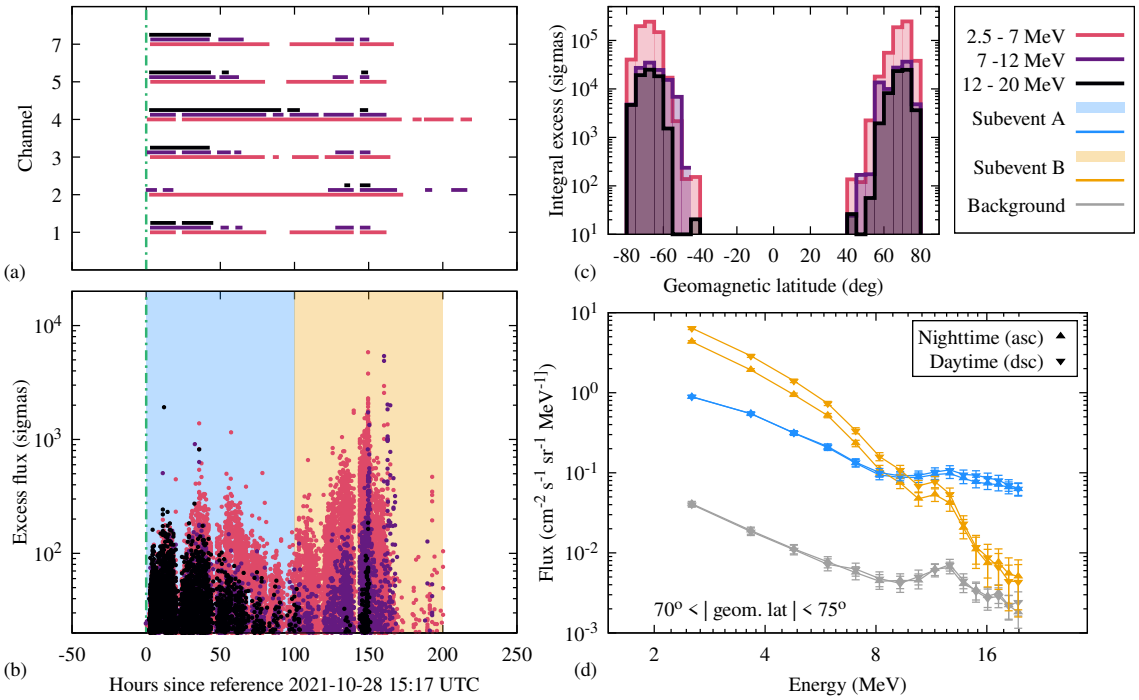

Figure 3: Features associated to the GLE of 2021-10-28. The meaning of colors is provided in the top right key. (a) Clusters detected for each channel and energy range. Each horizontal stripe is a cluster, covering the time span between the first and last outlier belonging to it. The vertical green dash-dotted line corresponds to the reference timestamp, 2021-10-28 15:17 UTC. (b) Outliers detected by all channels as a function of time. Each dot is an outlier, colored according to the energy range and whose ordinate value corresponds to the number of sigmas above the background. (c) Integral excess given by outliers (in number of sigmas over the background) as a function of the geomagnetic latitude. (d) Spectra of sub-events A and B (see panel (b)) compared to the background spectrum, for the geomagnetic latitude stripes between 70° and 75° in absolute value.

The plots of Fig. 3(a) and Fig. 3(b) suggest a time dependence of the energetic profile of the detected excess protons. This is quantitatively confirmed by the spectra of Fig. 3(d), obtained by dividing the time interval into two sub-events of 100 hours duration. While the spectrum of sub-event A is essentially an amplified version of the background one, the spectrum of sub-event B has a different shape, with a more prominent contribution of lower-energy particles.

4.2 X3.3 flare of 2023-02-09

The event starts with a X-3.3 flare with halo CME in region AR13575 at 2024-02-09 12:53 UTC. Between Feb. 08 and Feb. 12, fifteen subsequent M-class flares were detected. Figure 4 shows the detected outliers and clusters associated to this event, as well as the corresponding latitudinal distribution and spectra. The detected outliers cover about 60 hours after the reference UTC of the flare.

This event exhibits a prevalence of higher-energy particles in the excess proton flux, as one can evince by the relative abundance of black dots in Fig. 4(b). Indeed, the spectral shapes of Fig. 4(d)

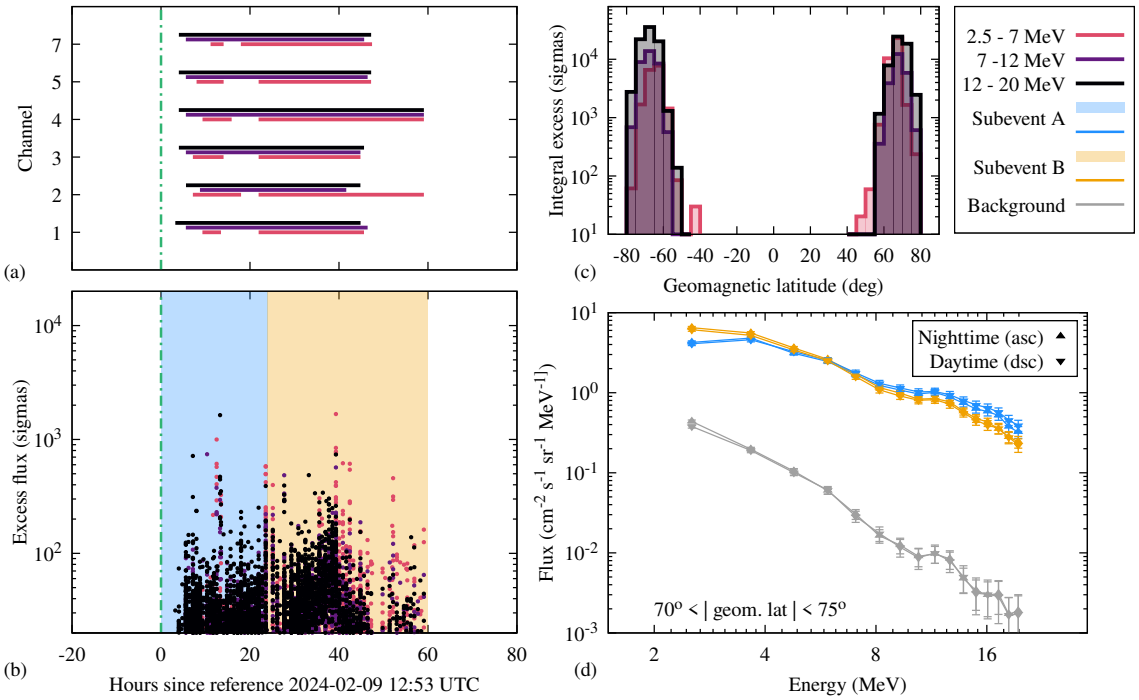

Figure 4: As in Fig. 3, but for the X3.3-class flare of 2024-02-09.

behave quite the opposite compared to Fig. 3: the high-energy end of the spectrum is amplified more than the lower-energy part.

5. Conclusions

The results of Figs. 3 and 4 showcase the capability of HEPP-L in providing valuable information on the development of long-lasting solar perturbations of the ionosphere. Specifically, the data provided by HEPP-L proved to be useful in both the identification of solar events by detecting anomalous fluxes, as well as in characterizing the spectral features of the event. As demonstrated by the two showcase events reported here, the energy resolution of HEPP-L allows to follow in detail the spectral evolution of the events, and to clearly distinguish different spectral behaviors between different events.

These results highlight the need for low-Earth observations in order to have a complete picture of the interaction of solar energetic particles and magnetic fields with the Earth's ionosphere, a key capability to study the dynamics of the near-Earth environment during geomagnetic storms [8]. Moreover, the information provided by the CSES constellation can play a crucial role in understanding and mitigating the hazardous effects of geomagnetic storms on satellites, communications, power infrastructures and on the human health [13, 14].

References

[1] Z. Zhima *et al.*, *The representative scientific results of the china seismo-electromagnetic satellite*, *Earthquake Research Advances* **5** (2025) 100314.

[2] S. Amoroso *et al.*, *Multispacecraft observations of the 27 day periodicity in galactic protons from 2018 to 2019*, *The Astrophysical Journal* **988** (2025) 181.

[3] R. Battiston *et al.*, *Observation of anomalous electron fluxes induced by grb221009a on cses-01 low-energy charged particle detector*, *The Astrophysical Journal Letters* **946** (2023) L29.

[4] S. Bartocci *et al.*, *The catalogue of gamma-ray burst observations by hepd-01 in the 0.3–50 mev energy range*, *The Astrophysical Journal* **976** (2024) 239.

[5] X.H. Shen *et al.*, *The state-of-the-art of the China Seismo-Electromagnetic Satellite mission*, *Science China Technological Sciences* **61** (2018) 634.

[6] F. Palma *et al.*, *The august 2018 geomagnetic storm observed by the High-Energy Particle Detector on board the CSES-01 satellite*, *Appl. Sci.* **11** (2021) 5680.

[7] M. Martucci *et al.*, *The first ground-level enhancement of solar cycle 25 as seen by the high-energy particle detector (hepd-01) on board the cses-01 satellite*, *Space Weather* **21** (2023) e2022SW003191.

[8] M. Piersanti *et al.*, *Comprehensive analysis of the geoeffective solar event of 21 june 2015: Effects on the magnetosphere, plasmasphere, and ionosphere systems*, *Solar Physics* **292** (2017) 169.

[9] X.Q. Li *et al.*, *The high-energy particle package onboard cses*, *Radiation Detection Technology and Methods* **3** (2019) 22.

[10] CSES-Limadou Collaboration collaboration, *Mapping the south atlantic anomaly charged particle environment with the hepd-01 detector on board the cses-01 satellite*, *Phys. Rev. D* **111** (2025) 022001.

[11] M. Steffen, *A simple method for monotonic interpolation in one dimension*, *Astronomy and Astrophysics* **239** (1990) 443.

[12] M. Ester, H. Kriegel, J. Sander and X. Xu, *A density-based algorithm for discovering clusters in large spatial databases with noise*, in *Proceedings of the Second International Conference on Knowledge Discovery and Data Mining*, KDD'96, p. 226–231, 1996.

[13] D.N. Baker, *Satellite anomalies due to space storms*, in *Space Storms and Space Weather Hazards*, I.A. Daglis, ed., (Dordrecht), pp. 285–311, Springer Netherlands (2001), DOI.

[14] A. Pulkkinen *et al.*, *Geomagnetically induced currents: Science, engineering, and applications readiness*, *Space Weather* **15** (2017) 828.

Full Authors List: CSES-Limadou collaboration

M. Babu[1,2], S. Bartocci[16], R. Battiston[1,2], S. Beolè[3,4], W. Burger[2], D. Campana[10], P. Cipollone[5], A. Contin[6,7], M. Cristoforetti[8,2], C. De Donato[5], C. De Santis[5], A. Di Luca[8,2], F. M. Follega[1,2], G. Gebbia[1,2], R. Iuppa[1,2], A. Lega[1,2], M. Lolli[7], M. Martucci[5], G. Masciantonio[5], M. Mergè[15], M. Mese[9,10], C. Neubüser[2], R. Nicolaidis[1,2], F. Nozzoli[2], A. Oliva[7], G. Osteria[10], F. Palma[5], B. Panico[9,10], F. Perfetto[10], A. Perinelli[1,2], S. Pietroni[11,5], P. Picozza[11,5], M. Pozzato[7], E. Ricci[1,2], L. Ricci[1,2], M. Ricci[5,12], S. B. Ricciarini[13], Z. Sahnoun[6,7], U. Savino[3,4], V. Scotti[9,10], M. Sorbara[11], A. Sotgiu[5], R. Sparvoli[11,5], P. Ubertini[14], V. Vilona[2], S. Zoffoli[15], P. Zuccon[1,2],

[1] Università di Trento, V. Sommarive 14, 38123 Povo (TN), Italy
[2] INFN - TIFPA, V. Sommarive 14, 38123 Povo (TN), Italy
[3] Università di Torino, Via P.Giuria 1, 10125, Turin, Italy
[4] INFN - Sezione di Torino, Via P.Giuria 1, 10125, Turin, Italy
[5] INFN - Sezione di Roma Tor Vergata, V. della Ricerca Scientifica 1, 00133, Rome, Italy
[6] Università di Bologna, V.le Berti Pichat 6/2, Bologna, Italy
[7] INFN - Sezione di Bologna, V.le Berti Pichat 6/2, Bologna, Italy
[8] Fondazione Bruno Kessler, Via Sommarive 18, 38123, Povo (TN), Italy
[9] Università degli Studi di Napoli Federico II, V. Cintia, 80126, Naples, Italy
[10] INFN - Sezione di Napoli, V. Cintia, 80126, Naples, Italy
[11] Università di Roma Tor Vergata, V. della Ricerca Scientifica 1, 00133, Rome, Italy
[12] INFN - LNF, V. E. Fermi 54, 00044 Frascati (RM), Italy
[13] IFAC-CNR, Via Madonna del Piano 10, 50019 Sesto Fiorentino (FI), Italy
[14] INAF-IAPS, V. Fosso del Cavaliere 100, 00133, Rome, Italy
[15] Italian Space Agency, V. del Politecnico, I-00133 Rome, Italy
[16] INFN – AC, Via E. Fermi 54, 00044 Frascati (RM), Italy

PoS(ICRC2025)1354